

The Noonan Syndrome Gene *Lztr1* Controls Cardiovascular Function by Regulating Vesicular Trafficking

Raj Nayan Sewduth^{1,2}, Silvia Pandolfi^{1,2}, Mikhail Steklov^{1,2}, Aidana Sheryazdanova^{1,2}, Peihua Zhao^{1,2}, Nathan Criem^{1,2}, Maria F. Baietti^{1,2}, Benoit Lechat^{1,2}, Rozeen Quarck³, Francis Impens^{4,5,6}, Anna A. Sablina^{1,2*}

¹ VIB-KU Leuven Center for Cancer Biology, VIB, Herestraat 49, 3000 Leuven, Belgium; ² Department of Oncology, KU Leuven, Herestraat 49, 3000 Leuven, Belgium; ³ University Hospitals and Department of Chronic Diseases, Metabolism & Ageing (CHROMETA), KU Leuven, Herestraat 49, 3000 Leuven, Belgium; ⁴ Department of Biomolecular Medicine, Ghent University, B-9000 Ghent, Belgium; ⁵ VIB Center for Medical Biotechnology, B-9000 Ghent, Belgium; ⁶ VIB Proteomics Core, Albert Baertsoenkaai 3, 9000 Ghent, Belgium.

Running Title: LZTR1 Loss Leads to Vascular Defects



Circulation Research

Subject Terms:

Animal Models of Human Disease
Angiogenesis
Genetically Altered and Transgenic Models
Vascular Disease

Address correspondence to:

Dr. Anna Sablina
Herestraat 49
3000 Leuven
Belgium
Tel: +32 16 37 69 27
anna.sablina@kuleuven.vib.be

ABSTRACT

Rationale: Noonan syndrome (NS) is one of the most frequent genetic disorders. Bleeding problems are among the most common, yet poorly defined complications associated with NS. A lack of consensus on the management of bleeding complications in NS patients indicates an urgent need for new therapeutic approaches.

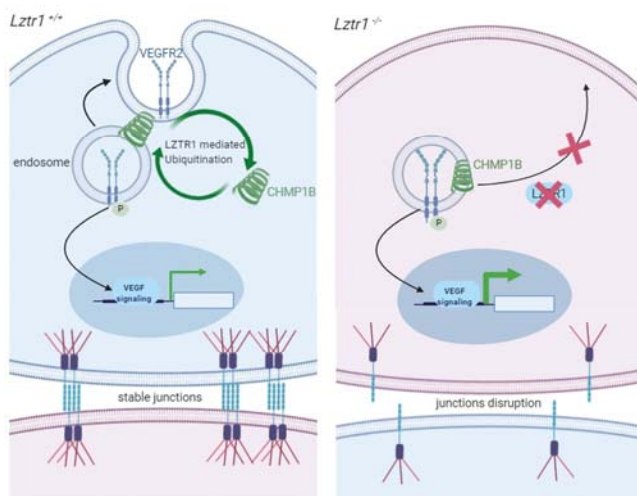
Objective: Bleeding disorders have recently been described in NS patients harboring mutations of LZTR1, an adaptor for CULLIN3 ubiquitin ligase complex. Here, we assessed the pathobiology of LZTR1-mediated bleeding disorders.

Methods and Results: Whole-body and vascular specific knockout of *Lztr1* results in perinatal lethality due to cardiovascular dysfunction. *Lztr1* deletion in blood vessels of adult mice leads to abnormal vascular leakage. We found that defective adherent and tight junctions in *Lztr1*-depleted endothelial cells are caused by dysregulation of vesicular trafficking. LZTR1 affects the dynamics of fusion and fission of recycling endosomes by controlling ubiquitination of the ESCRT-III component CHMP1B, whereas NS-associated *LZTR1* mutations diminish CHMP1B ubiquitination. LZTR1-mediated dysregulation of CHMP1B ubiquitination triggers endosomal accumulation and subsequent activation of VEGFR2 and decreases blood levels of soluble VEGFR2 in *Lztr1* haploinsufficient mice. Inhibition of VEGFR2 activity by cediranib rescues vascular abnormalities observed in *Lztr1* knockout mice

Conclusions: *Lztr1* deletion phenotypically overlaps with bleeding diathesis observed in NS patients. ELISA screening of soluble VEGFR2 in the blood of *LZTR1*-mutated NS patients may predict both the severity of NS phenotypes and potential responders to anti-VEGF therapy. VEGFR inhibitors could be beneficial for the treatment of bleeding disorders in NS patients

Keywords:

Noonan syndrome, cardiovascular disease, vesicular trafficking, LZTR1, hemorrhage, vascular function, ubiquitin, ubiquitin-proteasome system genetics, VEGF receptor.



Nonstandard Abbreviations and Acronyms:

Noonan Syndrome (NS)
Lewis lung carcinoma (LLC)
Endothelial cells (ECs)
Isolectin B4 (IB4)
mouse iG (miG)
empty vector (EV)
Cre-recombinase (Cre)
Wild-type (WT)
arbitrary units (AU).

INTRODUCTION

The incidence of Noonan Syndrome (NS) is reported to be between 1 in 1000 and 1 in 2500 births¹. NS is characterized by short stature, facial dysmorphism, and congenital heart defects². NS is also the first cause of nuchal translucency after Down Syndrome. Infants suffering from NS present varying degrees of symptoms, ranging from mild to life-threatening, including polyhydramnios, pleural effusions and edema^{3,4}.



Several studies have linked NS to lung lymphangiectasis, which is characterized by vessel dilatation, bronchiole collapse and hemorrhages⁵. It is usually associated with lung hypertension and can trigger pulmonary heart disease by affecting right ventricular function⁶. Between 50–89% of NS patients present bleeding disorders such as bruising and hemangioma⁷, whereas severe hemorrhages are observed in about 3% of cases⁸. Most of the studies describing the etiology of bleeding disorders in NS patients are incomplete. Coagulation defects, especially deficiencies of factors VIII, XI, XII and various combinations of these, have been documented in about 30% of NS patients. However, no consistent pattern of coagulation defects in NS has been established and many reports describe a poor correlation between bleeding history and clotting factor deficiencies⁷, indicating that the bleeding defects in NS patients are caused by other alterations.

An understanding of bleeding disorders in NS is clinically important because a large number of patients require surgery or take medication presenting bleeding as adverse effects, such as aspirin⁹. Currently, there is no consensus on the management of bleeding complications in patients with NS. Furthermore, conventional treatment including platelets and fresh frozen plasma do not appear to be efficient in NS¹⁰, demonstrating an urgent need for identification of new therapies for NS patients. NS is an autosomal dominant disease¹¹. In about half of the cases, the disease is caused by missense mutations in the *PTPN11* gene, resulting in a gain-of-function of the tyrosine phosphatase SHP2¹², whereas mutations in *SOS1*, *SOS2*, *RAF1*, *KRAS*, *NRAS*, *BRAF*, *SHOC2*, *CBL*, *RIT1* are found in NS patients at low rates. *LZTR1* has also been recently added to the list of genes causing NS and is present in up to 8% of NS patients^{13,14}. NS patients harboring *LZTR1* mutations presented the typical NS facial features, webbed neck, cardiovascular defects, and bleeding¹⁵.

LZTR1 serves as a substrate adaptor for CULLIN3 (CUL3) ubiquitin ligase complexes. In addition to NS, mutations in *LZTR1* have also been associated with glioblastoma¹⁶, hepatocarcinoma¹⁷, familial Schwannomatosis¹⁸, and pediatric cancers¹⁹. In our recent study, we demonstrated that knockout of *Lztr1* in mice leads to prenatal lethality, whereas *Lztr1* haploinsufficiency partially recapitulates NS phenotypes including facial dimorphism and heart malformations²⁰. As bleeding disorders are observed

in NS patients with different genotypes, we took advantage of conventional and vascular specific *Lztr1* knockout mouse models to characterize the vascular phenotypes triggered by *Lztr1* loss. The results of our study provide a fundamental explanation underlying the molecular mechanisms of endothelial dysfunction and etiology of the bleeding disorders in *Lztr1*-mutated NS as well as identify anti-VEGF therapies as a potential treatment approach for NS patients.

METHODS

Detailed experimental procedures, mouse models, cell culture and bioinformatics analysis are described in the Supplemental Materials in the Expanded Materials & Methods file. The materials used in this study are available from the corresponding author upon reasonable request. The RNAseq data generated for this study are available at GEO database with accession number GSE123044. The mass spectrometry data have been deposited to the ProteomeXchange Consortium via the PRIDE partner repository with the dataset identifier PXD011926.

RESULTS

Lztr1 loss leads to abnormal cardiovascular development.



To elucidate the etiology of bleeding disorders in *LZTR1*-mutated NS patients, we analyzed the whole-body *Lztr1* and the *Pdgfb*^{iCre ERT2}, *Lztr1*^{fl/fl} knockout mice. The *Pdgfb*^{iCre ERT2} model allows to target genes in the endothelium^{21,22} and is widely used to study vascular development during embryogenesis or disease progression^{23,24}. Vascular specific *Lztr1* knockout was induced by treating *Pdgfb*^{iCre ERT2}, *Lztr1*^{fl/fl} pregnant females with tamoxifen. Survival analysis demonstrated that both the whole-body and vascular specific knockouts of *Lztr1* led to embryonic lethality between E14.5 and E18.5 (Online Figure Ia, b). At E14.5, *Lztr1*^{-/-} embryos showed growth defects, hemorrhages, or significant hydrops, whereas *Lztr1*^{+/-} embryos did not show any obvious phenotypes (Figure 1a, b). Similarly, vascular specific *Lztr1* loss led to growth retardation, superficial hemorrhages, and edema (Figure 1c, d). In line with these findings, yolk sac vasculature of *Lztr1*^{-/-} embryos at that stage was dysfunctional as indicated by the presence of enlarged vascular structures (Figure 1e). Abnormal vascular leakage was also present in the cephalic plexus and skin vasculature (Figure 1b, d, f).

Lztr1 loss also caused pulmonary dysplasia. Histological analysis showed that *Lztr1*^{-/-} lungs presented narrower airspaces and discontinuous lung vessels (Online Figure 1c, d). SMA and CD31 immunostaining revealed disruption of the lung structure and vasculature in *Lztr1*^{-/-} embryos at E14.5 (Online Figure 1e). Vascular dysfunction might be partially responsible for the dysmorphic lung phenotype as it was also observed in *Pdgfb*^{iCre ERT2}, *Lztr1*^{fl/fl} embryos (Online Figure 1f, g).

Furthermore, we observed defective cardiac chamber maturation in E14.5 *Lztr1*^{-/-} embryos as indicated by a moderate decrease in ventricular wall thickness (Online Figure 1Ia), suggesting that cardiac failure could also be a possible cause of the *Lztr1*^{-/-} embryonic lethality. The defective cardiac maturation could also explain the cardiomyopathy phenotype previously described in adult *Lztr1*^{+/-} mice²⁰. Ventricular trabeculation and myocardial defects have been associated with endothelial dysfunction in other NS mice models²⁵. Concordantly, the heart of *Pdgfb*^{iCre ERT2}, *Lztr1*^{fl/fl} embryos displayed a striking non-compaction phenotype, as indicated by the hyper-trabeculation and decreased ventricular wall thickness (Online Figure 1Ib). These data indicate that *Lztr1* is essential for normal vascular function and subsequent coordination of lung alveolar and heart development.

Lztr1 loss in adult mice leads to cardiovascular dysfunction.

To examine the vascular phenotypes caused by *Lztr1* loss, we focused on the analysis of the adult *Lztr1*^{+/-} mice. We observed higher vessel density in the cardiac ventricles and relatively higher levels of phosphorylated Vascular Endothelial Growth Factor Receptor 2 (VEGFR2) in cardiac ventricle vessels of adult *Lztr1*^{+/-} mice (Online Figure IIc, d). Adult *Pdgfb*^{iCreERT2}, *Lztr1*^{fl/fl} mice injected with tamoxifen at weaning presented severe fibrosis in the right ventricle (Online Figure IIe), demonstrating the endothelial contribution to the severe cardiac dysfunction previously described in *Lztr1*^{+/-} mice²⁰.

Histological analyses also demonstrated that *Lztr1*^{+/-} animals presented multiple lung defects including vessel dilatation, pulmonary hemorrhages, and lung fibrosis (Figure 2a-d). Collectively, these results indicate that *Lztr1* inactivation partially recapitulates pulmonary and cardiovascular phenotypes commonly observed in NS patients presenting *LZTR1* mutations^{5,26}, indicating that the *Lztr1* knockout mice represent a clinically relevant model.

CD31 immunostaining showed that lung vessels in *Lztr1*^{+/-} mice were thinner and discontinuous (Figure 2e). Immunostaining of isolated endothelial cells (ECs) demonstrated that *Lztr1* haploinsufficiency led to abnormal adherent and tight junctions (Figure 2f; Online Figure IIff). The Evans blue extravasation assay revealed increased vascular permeability in the lungs of *Lztr1*^{+/-} mice (Figure 2g). We observed an even more striking increase in vascular permeability in the lungs and skin of *Pdgfb*^{iCreERT2}, *Lztr1*^{fl/fl} mice injected with tamoxifen at weaning (Figure 2h). In line with these findings, *Lztr1*^{+/-} sorted ECs were more permeable to 40 kDa Dextran when compared to *Lztr1*^{+/+} ECs (Figure 2i).



The observed phenotypes suggest a potential role of LZTR1 in the control of vascular function. Concordantly, aortic ring assay²⁷ demonstrated that *Lztr1*^{+/-} ECs were more neo-angiogenic as indicated by an increase in the sprouting area (Online Figure IIIa-c). To further assess the angiogenic potential of *Lztr1*^{+/-} ECs *in vivo*, we implanted Lewis lung carcinoma (LLC) cells²⁸ in the flanks of *Lztr1*^{+/+} and *Lztr1*^{+/-} mice. LLC tumors appeared earlier in *Lztr1*^{+/-} mice and displayed a higher weight at sacrifice (Online Figure III d, e). Histological analyses showed that LLC tumors in *Lztr1*^{+/-} mice were more vascularized and presented increased vascular leakage (Online Figure III f-i). Aortic ring assay using aortic rings isolated from *Pdgfb*^{iCreERT2}, *Lztr1*^{fl/fl} mice injected with tamoxifen at weaning also demonstrated that vascular specific loss of *Lztr1* was sufficient to increase neo-angiogenesis (Online Figure III j). These data indicate that *Lztr1* deletion disrupts the balance between vascular integrity and angiogenesis, leading to a more pro-angiogenic profile associated with less stable junctions.

LZTR1 controls endothelial function by regulating vesicular trafficking.

We next explored a potential mechanism by which *Lztr1* loss leads to a pro-angiogenic phenotype. In our recent study, we found that LZTR1 controls the activity of the RAS pathway²⁰. Indeed, we observed increased phosphorylation of ERK1/2 and AKT1 when we deleted *Lztr1* in *Lztr1*^{fl/fl} ECs derived from different mice by overexpressing *Cre*^{ERT2} recombinase (Online Figure IVa, b). However, the MEK1/2 inhibitor pimasertib, the AKT inhibitor ipatasertib, or the combination of both inhibitors only partially rescued the embryonic lethality phenotype, as upon either of the treatments we recovered *Lztr1*^{-/-} embryos at E18.5, but no pups at birth (Online Figure IVc). Treatment with pimasertib or ipatasertib did not rescue lung dysplasia in E18.5 *Lztr1*^{-/-} embryos. E18.5 *Lztr1*^{-/-} embryos treated with the combination of pimasertib and ipatasertib showed more moderate lung dysplasia, but still displayed massive lung hemorrhages, indicating that concurrent inhibition of MEK1/2 and AKT1 in *Lztr1*^{-/-} embryos could not restore normal lung vascular function (Online Figure IVd, e). Moreover, pimasertib, ipatasertib, or the combination of both inhibitors did not rescue the formation of abnormal adherent and tight junctions in *Lztr1*^{fl/fl}-*Cre*^{ERT2} ECs (Online Figure IVf). This suggests that *Lztr1* loss may contribute to human disease by additional mechanisms rather than the sole activation of the RAS pathway.

Using mass-spectrometry based approaches, we explored how *LZTR1* loss alters the proteome and ubiquitome landscapes. The Ingenuity Pathway Analysis (IPA) of either differentially expressed, or differentially ubiquitinated proteins in HeLa cells harboring wt-*LZTR1* or *LZTR1*-indels demonstrated that endocytosis was one of the top canonical pathways altered by *LZTR1* loss (Figure 3a, b). Several putative *LZTR1* interactors identified by the Virotrap approach²⁰ were also associated with vesicular trafficking (Figure 3c). Collectively, these data suggest a potential role of *LZTR1* in the regulation of vesicular trafficking.

To test this idea, we performed immunostaining of *LZTR1*-deleted cells for sorting nexin-1 (SNX1), a protein essential for early to late endosome trafficking. *Lztr1* knockout in *Lztr1^{fl/fl}* ECs infected with a *Cre^{ERT2}* recombinase led to abnormal endosomal tubulation, a phenotype associated with vesicular trafficking impairment (Figure 3d, e). Concordantly, SNX1-positive structures appeared spherical in wt-*LZTR1* HeLa cells, whereas *LZTR1* loss led to the accumulation of endosomal tubules (Online Figure Va). These results implicate *LZTR1* in the control of endosomal maturation and recycling^{29,30}.

To ascertain the role of *LZTR1* in vesicular trafficking, we performed a set of rescue experiments using the inhibitors of vesicular trafficking, Dynasore^{31,32} and Tyrphostin A23 (TyrA23)^{33,34}. Both treatments abolished the difference in the appearance of endosomal tubules between wt-*LZTR1* and *LZTR1*-deleted cells (Figure 3d, e; Online Figure Va). Furthermore, both inhibitors normalized adherent and tight junctions in *Lztr1^{fl/fl}*-*Cre^{ERT2}* ECs (Figure 3f, g). Depletion of *Dynamin 1* with a siRNA (Online Figure IVg) also restored normal junctions in *Lztr1^{fl/fl}*-*Cre^{ERT2}* ECs (Online Figure IVg, h, i). Prenatal treatment with Dynasore partially rescued the embryonic lethality phenotype caused by *Lztr1* knockout, as we observed a nearly normal ratio of *Lztr1^{-/-}* embryo at E18.5, but not at birth (Figure 3h). In contrast to the treatment with either pimasetrib or ipatasertib, Dynasore recovered lung dysplasia in E18.5 *Lztr1^{-/-}* embryos (Online Figure IVd, e). Together, these results indicate that *LZTR1*-mediated vascular dysfunction could be explained by defects in vesicular trafficking.

LZTR1 controls ubiquitination of the ESCRT-III component CHMP1B.

We next assessed the molecular mechanism by which *LZTR1* is implicated in vesicular trafficking. The component of ESCRT-III (endosomal sorting complex required for transport III) trafficking machinery, CHarged Multivesicular Proteins 1B (CHMP1B), was present among both the putative *LZTR1* interactors identified by the Virotrap screen²⁰. CHMP1B also showed one of the highest scores in the fold change ranking when we compared ubiquitination landscapes of wt-*LZTR1* and *LZTR1*-indel cells. Apart from the lysine 6 site, all CHMP1B ubiquitination sites (lysines 42, 59, 87, 90, 104, and 110) showed at least a two-fold decrease in *LZTR1*-indel cells (Figure 4a). This suggests that *LZTR1* might regulate vesicle trafficking by controlling CHMP1B ubiquitination.

We confirmed the interaction of endogenous CHMP1B and HA-tagged *LZTR1* using co-immunoprecipitation (Figure 4b, c). Of note, CHMP1B forms homo- and heteromers and is detected in cell lysates as a monomer (28kDa), a dimer (55kDa), and a multimer even under denaturing conditions, which is consistent with previously published results³⁵. Moreover, a recent report demonstrated that stimulation with growth factors or cytokines promotes CHMP1B ubiquitination³⁵. Concordantly to this observation, we found increased binding of *LZTR1* to CHMP1B in ECs upon stimulation with VEGF (Figure 4d). On the other hand, treatment with the CULLIN neddylation inhibitor MLN4924, which blocks the activity of the *LZTR1*/CUL3 complex, did not affect the interaction between *LZTR1* and CHMP1B, indicating that their binding does not depend on the ubiquitination status of CHMP1B (Figure 4d).

We then assessed *LZTR1* contribution to the control of CHMP1B ubiquitination. CHMP1B was present in mono- or multi-ubiquitinated forms. This is consistent with the mass-spectrometry results showing ubiquitination of CHMP1B at seven different lysines. Substitution of 7 lysines to arginines abolished CHMP1B ubiquitination (Online Figure Vb). We found that *LZTR1*-indel in HeLa cells also led

to decreased ubiquitination of V5-tagged wild-type and endogenous CHMP1B (Online Figure Vc). Moreover, we observed lower levels of CHMP1B ubiquitination upon *Lztr1* knockout in mice when comparing *Lztr1*^{+/+} and *Lztr1*^{+/-} yolk sacs; *Lztr1*^{+/+} and *Lztr1*^{+/-} sorted ECs; and *Lztr1*^{fl/fl} ECs expressing an empty vector (EV) or *Cre*^{ERT2} recombinase (Figure 4e; Online Figure Vd, e). Increased binding of LZTR1 to CHMP1B upon VEGF stimulation in ECs was associated with increased levels of ubiquitinated CHMP1B, whereas MLN4924 treatment abolished VEGF-induced CHMP1B ubiquitination (Figure 4f), further confirming that LZTR1 controls CHMP1B ubiquitination in a Cullin-dependent manner.

Noonan-associated LZTR1 mutations diminish the ability of LZTR1 to ubiquitinate CHMP1B.

We examined whether Noonan Syndrome associated phenotypes could be also be associated with the impaired ability of mutated LZTR1 to control CHMP1B ubiquitination. Both truncated and missense mutations of LZTR1 have been reported in Noonan Syndrome. Missense mutations of *LZTR1* are spread throughout the whole gene^{13,36,37}. In our recent study, we found that LZTR1 mutations within the BTB (broad-complex, tramtrack and bric-a-brac)-BACK domains abolish the formation of the LZTR1/CUL3 complex, suggesting that the BTB-BACK LZTR1 mutations abolish ubiquitination of all LZTR1 substrates²⁰. On the other hand, LZTR1 mutations within the Kelch domain, which is responsible for the substrate binding, might diminish the ability of LZTR1 to ubiquitinate CHMP1B by affecting the interaction between LZTR1 and CHMP1B. Therefore, we tested the ability of the Kelch domain LZTR1 mutants to bind and ubiquitinate CHMP1B. We found that all Kelch domain LZTR1 mutations, except for M202R, showed decreased ability to interact with CHMP1B (Figure 4b, c). Importantly, three LZTR1 mutations, R97L, N145L and R284C, observed in NS patients showing bleeding phenotype^{38,39}, caused the inability of LZTR1 to ubiquitinate CHMP1B (Figure 4g). This suggests that dysregulation of CHMP1B ubiquitination could be associated with the bleeding disorders observed in *LZTR1*-mutated Noonan Syndrome patients.

Dysregulation of LZTR1-mediated ubiquitination of CHMP1B impedes vesicle trafficking.

Our next question was how dysregulation of LZTR1-mediated ubiquitination of CHMP1B affects vesicular trafficking. The most well-described function of CHMP1B is to promote the formation of recycling tubules from endosomes⁴⁰ by co-assembling with the other ESCRT-III component increased sodium tolerance I (ISTI)^{41,42}. Indeed, *Chmp1b* depletion led to the dysregulation of recycling trafficking as we detected an accumulation of RAB11-positive recycling endosomes (Figure 5a, b). *Lztr1* knockout in ECs presented a similar accumulation of RAB11-positive endosomes. We also found an accumulation of CHMP1B/RAB11-positive recycling endosomes in *Lztr1*^{+/-} ECs and *Lztr1*^{fl/fl} ECs infected with a *Cre*^{ERT2} recombinase (Figure 5c, d, e). In contrast, we did not observe an increase of CHMP1B in early EAA1-positive or late LAMP1-positive endosomes (Figure 5d, e). On the other hand, suppression of *Chmp1b* in *Lztr1*^{-/-} ECs did not affect the localization of RAB11 (Figure 5a, b), suggesting that the effect of CHMP1B on trafficking is LZTR1 dependent.

We further confirmed the effect of LZTR1-mediated CHMP1B ubiquitination on vesicle trafficking by rescue experiments. Whereas suppression of *CHMP1B* led to the accumulation of RAB11-positive vesicles, overexpression of wild-type CHMP1B restored the trafficking of recycling endosomes. On the other hand, ubiquitination-deficient CHMP1B-7K>R mutant did not rescue the accumulation of RAB11-positive endosomes triggered by CHMP1B depletion. Finally, modulation of CHMP1B expression in *LZTR1*-indels cells showed no effect on recycling endosome trafficking (Figure 5f, Online Figure Vf, g), indicating that LZTR1-mediated ubiquitination of CHMP1B plays a crucial role in vesicular trafficking.

We also assessed the mechanism by which LZTR1-mediated ubiquitination of CHMP1B affects its functioning. Consistently to a recent study³⁵, we did not observe any degradative poly-ubiquitination of CHMP1B (Figure 4e, f; Online Figure Vb-e). On the other hand, it was reported that USP8-mediated

deubiquitination of CHMP1B promotes its co-assembly with IST1³⁵. In line with this observation, *LZTR1* loss increased the interaction between CHMP1B and IST1 (Online Figure Vh). Collectively, these results indicate that *LZTR1* loss affects recycling trafficking by abolishing CHMP1B ubiquitination and dysregulating the assembly of the CHMP1B/ IST1 complex, a key component of the ESCRTIII complex necessary for endosomal trafficking.

Lztr1 loss activates the VEGF pathway by dysregulating VEGFR2 trafficking.

As a component of the ESCRT-III complex, CHMP1B is implicated in the trafficking of stimulated growth factor receptors, suggesting that LZTR1-mediated dysregulation of CHMP1B could affect receptor signaling. Consistent with this idea, the timing of VEGF-induced CHMP1B ubiquitination coincides with the onset of VEGFR2 internalization and activation (Figure 4d, f), suggesting that CHMP1B ubiquitination might regulate VEGFR2 trafficking. Moreover, we observed higher levels of phosphorylated VEGFR2 in *Lztr1*^{-/-} heart vessels, suggesting that LZTR1 might contribute to the regulation of VEGFR2 activity (Online Figure IId). The IPA Upstream Regulator Analysis of genes differentially expressed in *Lztr1*^{+/+} and *Lztr1*^{+/-} MEFs also predicted VEGF activation of in *Lztr1* knockout cells (Online Figure VIa). Besides, the VEGF/ VEGFR2 pathway plays a central role in endothelial cell function; and among the angiogenic drugs, the VEGFR2 specific inhibitors have produced notable results in different diseases⁴³⁻⁴⁵. Therefore, we decided to specifically focus on VEGF signaling.

We assessed the effect of *Lztr1* on the intracellular localization of VEGFR2 by performing immunocytochemistry analysis of VEGFR2 in ECs with or without permeabilization. Whereas VEGFR2 was strongly expressed on the cell surface of *Lztr1*^{+/+} ECs, we detected less VEGFR2 signal on the surface of *Lztr1*^{+/-} ECs (Online Figure VIb, c). On the other hand, we observed an accumulation of VEGFR2 on RAB11/ CHMP1B-positive vesicles in *Lztr1*-deleted ECs (Figure 6a-c). A similar accumulation of VEGFR2 on endosomes was observed in *Chmp1b*-depleted cells, indicating abnormal trafficking of the receptor (Figure 5a; Figure 6c). It has been recently reported that the constitutive VEGFR2 internalization protects the receptor against ectodomain cleavage⁴⁶, suggesting that *Lztr1* loss might result in decreased VEGFR2 shedding. Indeed, ELISA analysis revealed lower levels of soluble VEGFR2 in the blood serum of *Lztr1*^{+/-} mice (Figure 6d). Treatment with Dynasore or TyrA23 abolished endosomal accumulation of VEGFR2 in *Lztr1*^{+/-} ECs (Figure 6a, b). *Dynammin 1* suppression also reduced internalization of the receptor in *Lztr1*^{fl/fl} ECs expressing *Cre*^{ERT2} (Online Figure VIId, e). Altogether, these results indicate that dysregulation of LZTR1-mediated ubiquitination of CHMP1B could play a critical role in the regulation of VEGFR2 trafficking.

Because internalization and phosphorylation of the VEGFR2 complex are hallmarks of VEGF signaling activation^{47,48}, we hypothesized that LZTR1-mediated dysregulation of VEGFR2 trafficking might lead to its activation. Concordantly, we detected a higher level of phosphorylated VEGFR2 in *Lztr1*^{+/-} ECs and *Lztr1*^{+/-} yolk sacs (Online Figure VI f, g, i). *Lztr1* knockout in *Lztr1*^{fl/fl} ECs by overexpressing *Cre*^{ERT2} recombinase also led to increased levels of VEGFR2 phosphorylation (Online Figure VI h, i). Suppression of *Dynammin 1* expression partially rescued increased levels of VEGFR2 phosphorylation in *Lztr1*-depleted cells (Online Figure VI k). VEGFR2 activation was CULLIN-dependent as MLN4924 abolished the accumulation of phosphorylated VEGFR2 (Figure 6d, e). TyrA23 treatment partially rescued VEGFR2 activation in *Lztr1* knockout ECs, indicating that increased VEGFR2 activity is due to dysregulated endosomal trafficking (Figure 6e, f).

To assess whether enhanced VEGFR signaling is responsible for the vascular phenotypes in *Lztr1* knockout mice, we blocked VEGFR2 activity in *Lztr1*^{fl/fl}-*Cre*^{ERT2} ECs with cediranib^{49,50}. Cediranib treatment normalized adherent and tight junctions (Figure 6g, h), confirming that *Lztr1* deletion affects junctional integrity through VEGFR activation. Furthermore, VEGF treatment significantly increased Evans blue extravasation in the skin of *Lztr1*^{fl/fl} mice, but only moderately in *Pdgfb*^{CreERT2}, *Lztr1*^{fl/fl} mice,

confirming that the pathway is already activated in *Lztr1* deleted cells (Figure 6i). Importantly, blocking of VEGFR2 activity with cediranib normalized tight and adherent junctions and rescued vascular leakage in the skin of *Pdgfb^{iCreERT2}, Lztr1^{fl/fl}* mice (Figure 6j). Altogether, these data indicate that loss of *Lztr1* leads to the up-regulation of VEGFR2 signaling by dysregulating vesicular trafficking, thus implying that blocking the catalytic activity of VEGFR could be advantageous for NS patients.

DISCUSSION

Nearly two-thirds of NS patients exhibit clinical signs of a bleeding diathesis that may manifest with easy bruising, postoperative bleeding complications, and rarely spontaneous hemorrhages²⁶. Here we explored the role of *LZTR1*, a gene recently linked to NS development, in the regulation of vascular function. We found that *Lztr1* whole-body knockout mice died *in utero*, suffering from severe hemorrhages and in some cases, hydrops. This is in line with previous observations from other NS models^{25,51}. Similarly, *Ptpn11D61G* and *Sos1E846K* embryos show hemorrhages at E13.5^{51,52}. *Lztr1* haploinsufficiency in adult mice also partially recapitulates bleeding phenotypes observed in NS patients, especially in the context of novel studies making the link between *Lztr1* mutations and coagulation defects^{38,39}.

Patients with *PTPN11* mutations show an increased prevalence of bleeding disorders compared with those having other mutations⁵³. On the other hand, bleeding disorders in NS appear to be least correlated with *KRAS* and *RAF1* mutations^{1,54}. This suggests that bleeding phenotypes might be associated with RAS-independent functions of the NS genes. Concordantly to this idea, *PTPN11*, which encodes the protein tyrosine phosphatase SHP-2, protects endothelial barrier through VE-cadherin stabilization⁵⁵. Here, we also found that MEK1/2 inhibition does not rescue vascular dysfunction induced by *Lztr1* loss. Unbiased proteome and ubiquitome analyses revealed that endocytosis is one of the top canonical pathways altered by *Lztr1* loss. Importantly, treatment with either Dynasore, TyrA23 or *dynamain 1* siRNA rescues endothelial dysfunction mediated by *Lztr1* loss, confirming that *LZTR1*-mediated vascular phenotypes are caused by dysregulation of vesicular trafficking.

Unbiased interaction screen and ubiquitome analysis indicate that the key component of the ESCRT III complex CHMP1B could be a direct substrate of the *LZTR1/ CUL3* complex. A previous study demonstrated that decreased ubiquitination of CHMP1B appears to block membrane fission by affecting its interaction with IST1⁵⁶. Concordantly, *LZTR1* loss appears to reduce CHMP1B ubiquitination on lysine residues important for its interaction with IST1^{41,42}. CHMP1B and IST1 form a 3D structure that gives the plasticity to membrane invagination required for the fusion and fission of vesicles. In fact, *LZTR1* loss strengthens the binding of CHMP1B to IST1, resulting in inhibition of membrane fission. Therefore, we could speculate that *LZTR1*-triggered defects in vesicular trafficking might be due to the dysregulation of the interaction between CHMP1B and IST1 that may affect the disassembly of the ESCRT-III complex. Importantly, all *LZTR1* mutations found in NS patients with bleeding disorders led to a decreased ability to interact with CHMP1B. Nonetheless, we could not exclude the possibility that *LZTR1* might modulate other regulators of vesicular trafficking.

Dysregulation of vesicle trafficking might lead to the activation of several receptor pathways⁵⁷. Here, we demonstrated that *Lztr1* loss activates VEGFR2 signaling, which is the primary tyrosine kinase receptor transmitting VEGF signals to control the balance between endothelial plasticity and junctional stability. Increased internalization and phosphorylation of VEGFR2 in Clathrin-dependent vesicles led to the activation of angiogenesis and increased endothelial permeability^{32,58}. Therefore, the *Lztr1*-mediated bleeding phenotypes could be at least partially explained by the activation of VEGF signaling. Consistent with this idea, overexpression of VEGF-A results in severe endothelial dysfunction, such as abnormal

angiogenesis and vascular leakage during development^{59,60}, leading to the accumulation of endocytic vesicles containing active VEGFR2.

Even though inhibition of the MAPK and PI3K/AKT pathways did not rescue endothelial dysfunction observed in *Lztr1* knockout mice, VEGFR2 led to the activation of multiple signaling pathways⁶¹. As an example, VEGFR2 recruits the adaptor protein Nck adaptor protein 1 (NCK1) and the SRC family tyrosine kinase FYN. NCK1/FYN complex formation regulates phosphorylation of PAK2, which in turn activates CDC42 and p38 MAPK, leading to actin remodeling. Recruitment of PLC γ 1 and SH2-domain-containing adaptor protein B (SHB) by VEGFR2 facilitates the interaction with FAK (focal adhesion kinase) and contributes to endothelial cell migration and attachment. SHB activation of PI3K induces endothelial nitric oxide (NO) synthase (eNOS) that promotes cell survival and NO-induced vascular permeability respectively.

Current treatments for NS patients suffering from bleeding including platelets and fresh frozen plasma do not appear to be efficient in NS¹⁰. Several anti-VEGF approaches have been recently validated to limit blood loss, including angiogenesis inhibitors such as bevacizumab, an antibody targeting Vascular Endothelial Growth Factor (VEGF), cediranib⁶²⁻⁶³ or thalidomide⁶⁴. Our results strongly indicate that inhibiting the catalytic activity of VEGF receptors could be beneficial to reduce bleeding in NS patients. Moreover, we found that *Lztr1* loss leads to increased levels of soluble VEGFR2 in blood serum, suggesting that ELISA-based screening of NS patients for the blood levels of soluble VEGFR2 might allow predicting potential responders to anti-VEGF therapy. Collectively, our results provide a potential explanation for the role of LZTR1 in vascular function and suggest novel therapeutic approaches for NS patients.



AUTHOR CONTRIBUTION

RS, SP and BL performed mice experiments; RS performed biochemical, cellular and immunostaining experiments; AS generated cell lines; NC performed the molecular cloning; BL performed the mouse genotyping; FI and MS performed the proteomics experiments; FI and PZ performed the bioinformatics analysis; RS and AAS designed the study; RS, NC, MFB, and AAS analyzed the data and wrote the manuscript. All authors discussed the results and commented on the manuscript.

DISCLOSURES

The authors claim no conflict of interest.

SOURCES OF FUNDING

This work was supported by H2020 European Research Council (ub-RASDisease) and Fonds Wetenschappelijk Onderzoek Research project G068715N.

SUPPLEMENTAL MATERIALS

Expanded Materials & Methods
Major Resources Table
Online Figures I – VI
Uncropped Blots

REFERENCES

1. Roberts AE, Allanson JE, Tartaglia M, Gelb BD. Noonan syndrome. *Lancet*. 2013;381:333-342. doi:10.1016/S0140-6736(12)61023-X
2. Sznajder Y, Keren B, Baumann C, et al. The spectrum of cardiac anomalies in Noonan syndrome as a result of mutations in the PTPN11 gene. *Pediatrics*. 2007;119:e1325-31. doi:10.1542/peds.2006-0211
3. Bakker M, Pajkrt E, Mathijssen IB, Bilardo CM. Targeted ultrasound examination and DNA testing for Noonan syndrome, in fetuses with increased nuchal translucency and normal karyotype. *Prenat Diagn*. 2011;31:833-840. doi:10.1002/pd.2782
4. Nisbet DL, Griffin DR, Chitty LS. Prenatal features of Noonan syndrome. *Prenat Diagn*. 1999;19:642-647. doi:10.1002/(SICI)1097-0223(199907)19:7<642::AID-PD610>3.0.CO;2-1
5. Hernandez RJ, Rosenthal A. Pulmonary Lymphangiectasis in Noonan Syndrome. *AJR*. 1980;134:75-80. doi: 10.2214/ajr.134.1.75
6. Witt DR, Hoyme HE, Zonana J, et al. Lymphedema in Noonan syndrome: Clues to pathogenesis and prenatal diagnosis and review of the literature. *Am J Med Genet*. 1987;27:841-856. doi:10.1002/ajmg.1320270412
7. Nugent DJ, Romano AA, Sabharwal S, Cooper DL. Evaluation of bleeding disorders in patients with Noonan syndrome: A systematic review. *J Blood Med*. 2018;9:185-192. doi:10.2147/JBM.S164474
8. Massarano A, Wood A, Tait R, Stevens R, Super M. Noonan syndrome: coagulation and clinical aspects. *Acta Paediatr*. 2010;85:1181-1185. doi:10.1111/j.1651-2227.1996.tb18225.x
9. Sharland M, Patton MA, Talbot S, Chitolie A, Bevan DH. Coagulation-factor deficiencies and abnormal bleeding in Noonan's syndrome. *Lancet*. 1992;339:19-21. doi:10.1016/0140-6736(92)90141-O
10. Tofil NM, Winkler MK, Watts RG, Noonan J. The use of recombinant factor VIIa in a patient with Noonan syndrome and life-threatening bleeding. *Pediatr Crit Care Med*. 2005;6:352-354. doi:10.1097/01.PCC.0000160656.71424.D1
11. Tartaglia M, Gelb BD, Zenker M. Noonan syndrome and clinically related disorders. *Best Pract Res Clin Endocrinol Metab*. 2011;25:161-179. doi:10.1016/j.beem.2010.09.002
12. Tartaglia M, Mehler EL, Goldberg R, et al. Mutations in PTPN11, encoding the protein tyrosine phosphatase SHP-2, cause Noonan syndrome. *Nat Genet*. 2001;29:465-468. doi:10.1038/ng772
13. Johnston JJ, van der Smagt JJ, Rosenfeld JA, et al. Autosomal recessive Noonan syndrome associated with biallelic LZTR1 variants. *Genet Med*. 2018;20:1175-1185. doi:10.1038/gim.2017.249
14. Nakaguma M, Jorge AAL, Arnhold IJP. Noonan syndrome associated with growth hormone deficiency with biallelic LZTR1 variants. *Genet Med*. 2019;21:260. doi:10.1038/s41436-018-0041-5
15. Aoki Y, Niihori T, Inoue SI, Matsubara Y. Recent advances in RASopathies. *J Hum Genet*. 2016;61:33-39. doi:10.1038/jhg.2015.114
16. Frattini V, Trifonov V, Chan JM, et al. The integrated landscape of driver genomic alterations in glioblastoma. *Nat Genet*. 2013;45:1141-1149. doi:10.1038/ng.2734
17. Ally A, Balasundaram M, Carlsen R, et al. Comprehensive and Integrative Genomic Characterization of Hepatocellular Carcinoma. *Cell*. 2017;169:1327-1341.e23. doi:10.1016/j.cell.2017.05.046
18. Paganini I, Chang VY, Capone GL, et al. Expanding the mutational spectrum of LZTR1 in schwannomatosis. *Eur J Hum Genet*. 2015;23:963-968. doi:10.1038/ejhg.2014.220
19. Ruggieri M, Praticò AD, Evans DG. Diagnosis, Management, and New Therapeutic Options in Childhood Neurofibromatosis Type 2 and Related Forms. *Semin Pediatr Neurol*. 2015;22:240-258. doi:10.1016/j.spen.2015.10.008
20. Steklov M, Pandolfi S, Baietti MF, et al. Mutations in LZTR1 drive human disease by dysregulating RAS ubiquitination. *Science*. 2018;362:1177-1182. doi:10.1126/science.aap7607

21. Claxton S, Kostourou V, Jadeja S, Chambon P, Hodivala-Dilke K, Fruttiger M. Efficient, inducible cre-recombinase activation in vascular endothelium. *Genesis*. 2008;46:74-80. doi:10.1002/dvg.20367
22. Hellström M, Gerhardt H, Kalén M, et al. Lack of pericytes leads to endothelial hyperplasia and abnormal vascular morphogenesis. *J Cell Biol*. 2001;152:543-553. doi:10.1083/jcb.153.3.543
23. Sewduth RN, Jaspard-Vinassa B, Peghaire C, et al. The ubiquitin ligase PDZRN3 is required for vascular morphogenesis through Wnt/planar cell polarity signalling. *Nat Commun*. 2014;5:4832. doi:10.1038/ncomms5832
24. Sewduth RN, Kovacic H, Jaspard-Vinassa B, et al. PDZRN3 destabilizes endothelial cell-cell junctions through a PKC ζ -containing polarity complex to increase vascular permeability. *Sci Signal*. 2017;10:eag3209. doi:10.1126/scisignal.aag3209
25. Lauriol J, Cabrera JR, Roy A, et al. Developmental SHP2 dysfunction underlies cardiac hypertrophy in Noonan syndrome with multiple lentigines. *J Clin Invest*. 2016;126:2989-3005. doi:10.1172/JCI80396
26. Artoni A, Selicorni A, Passamonti SM, et al. Hemostatic Abnormalities in Noonan Syndrome. *Pediatrics*. 2014;133:e1299-e1304. doi:10.1542/peds.2013-3251
27. Baker M, Robinson SD, Lechertier T, et al. Use of the mouse aortic ring assay to study angiogenesis. *Nat Protoc*. 2012;7:89-104. doi:10.1038/nprot.2011.435
28. Futakuchi M. Animal Model of Lung Metastasis of Hepatocellular Carcinoma: A Tool for the Development of Anti-Metastatic Therapeutics. *J Cancer Ther*. 2013;04:420-425. doi:10.4236/jct.2013.42A051
29. Newton TM, Reid E. An automated image analysis system to quantify endosomal tubulation. *PLoS One*. 2016;11:1-11. doi:10.1371/journal.pone.0168294
30. Bryant DM, Kerr MC, Hammond LA, et al. EGF induces macropinocytosis and SNX1-modulated recycling of E-cadherin. *J Cell Sci*. 2007;120:1818-1828. doi:10.1242/jcs.000653
31. Preta G, Cronin JG, Sheldon IM. Dynasore - Not just a dynamin inhibitor. *Cell Commun Signal*. 2015;13:1-7. doi:10.1186/s12964-015-0102-1
32. Basagiannis D, Zografou S, Galanopoulou K, Christoforidis S. Dynasore impairs VEGFR2 signalling in an endocytosis-independent manner. *Sci Rep*. 2017;7:1-11. doi:10.1038/srep45035
33. Stahlschmidt W, Robertson MJ, Robinson PJ, McCluskey A, Haucke V. Clathrin terminal domain-ligand interactions regulate sorting of mannose 6-phosphate receptors mediated by AP-1 and GGA adaptors. *J Biol Chem*. 2014;289:4906-4918. doi:10.1074/jbc.M113.535211
34. Robertson MJ, Deane FM, Stahlschmidt W, et al. Synthesis of the Pitstop family of clathrin inhibitors. *Nat Protoc*. 2014;9:1592-1606. doi:10.1038/nprot.2014.106
35. Crespo-Yañez X, Aguilar-Gurrieri C, Jacomin AC, et al. CHMP1B is a target of USP8/UBPY regulated by ubiquitin during endocytosis. *PLoS Genet*. 2018;14:1-24. doi:10.1371/journal.pgen.1007456
36. Ghedira N, Kraoua L, Lagarde A, et al. Further Evidence for the Implication of LZTR1 , a Gene Not Associated with the Ras-Mapk Pathway, in the Pathogenesis of Noonan Syndrome. *Biol Med*. 2017;9:4-7. doi:10.4172/0974-8369.1000414
37. Umeki I, Niihori T, Abe T, Nobuhiko K, Seiji O. Delineation of LZTR1 mutation-positive patients with Noonan syndrome and identification of LZTR1 binding to RAF1 – PPP1CB complexes. *Hum Genet*. 2018;138:21-35. doi:10.1007/s00439-018-1951-7
38. Pagnamenta AT, Kaisaki PJ, Bennett F, et al. Delineation of dominant and recessive forms of LZTR1-associated Noonan syndrome. *Clin Genet*. 2019;95:693-703. doi:10.1111/cge.13533
39. Jacquinet A, Bonnard A, Capri Y, et al. Oligo-astrocytoma in LZTR1-related Noonan syndrome. *Eur J Med Genet*. 2020;63:103617. doi:10.1016/j.ejmg.2019.01.007
40. Allison R, Lumb JH, Fassier C, et al. An ESCRT-spastin interaction promotes fission of recycling tubules from the endosome. *J Cell Biol*. 2013;202:527-543. doi:10.1083/jcb.201211045
41. McCullough J, Clippinger AK, Talledge N, et al. Structure and membrane remodeling activity of ESCRT-III helical polymers. *Science*. 2015;350:1548-1551. doi:10.1126/science.aad8305



42. Bajorek M, Schubert HL, McCullough J, et al. Structural basis for ESCRT-III protein autoinhibition. *Nat Struct Mol Biol.* 2009;16:754-762. doi:10.1038/nsmb.1621
43. Park MS, Ravi V, Araujo DM. Inhibiting the VEGF-VEGFR pathway in angiosarcoma, epithelioid hemangioendothelioma, and hemangiopericytoma/solitary fibrous tumor. *Curr Opin Oncol.* 2010;22:351-355. doi:10.1097/CCO.0b013e32833aaad4
44. Kodack DP, Chung E, Yamashita H, et al. Combined targeting of HER2 and VEGFR2 for effective treatment of HER2-amplified breast cancer brain metastases. *Proc Natl Acad Sci U S A.* 2012;109: e3119-27. doi:10.1073/pnas.1216078109
45. Pandey AK, Singhi EK, Arroyo JP, et al. Mechanisms of VEGF (vascular endothelial growth factor) inhibitor-associated hypertension and vascular disease. *Hypertension.* 2018;71:e1-e8. doi:10.1161/HYPERTENSIONAHA.117.10271
46. Basagiannis D, Christoforidis S. Constitutive endocytosis of VEGFR2 protects the receptor against shedding. *J Biol Chem.* 2016;291:16892-16903. doi:10.1074/jbc.M116.730309
47. Sawamiphak S, Seidel S, Essmann CL, et al. Ephrin-B2 regulates VEGFR2 function in developmental and tumour angiogenesis. *Nature.* 2010;465:487-491. doi:10.1038/nature08995
48. Genet G, Boyé K, Mathivet T, et al. Endophilin-A2 dependent VEGFR2 endocytosis promotes sprouting angiogenesis. *Nat Commun.* 2019;10:1-15. doi:10.1038/s41467-019-10359-x
49. Medinger M, Esser N, Zirrgiebel U, Ryan A, Jürgensmeier JM, Drevs J. Antitumor and antiangiogenic activity of cediranib in a preclinical model of renal cell carcinoma. *Anticancer Res.* 2009;29:5065-5076.
50. Brave SR, Ratcliffe K, Wilson Z, et al. Assessing the activity of cediranib, a VEGFR-2/3 tyrosine kinase inhibitor, against VEGFR-1 and members of the structurally related PDGFR family. *Mol Cancer Ther.* 2011;10:861-873. doi:10.1158/1535-7163.MCT-10-0976
51. Araki T, Mohi MG, Ismat FA, et al. Mouse model of Noonan syndrome reveals cell type- and gene dosage-dependent effects of Ptpn11 mutation. *Nat Med.* 2004;10:849-857. doi:10.1038/nm1084
52. Uhlén P, Burch PM, Zito CI, Estrada M, Ehrlich BE, Bennett AM. Gain-of-function/Noonan syndrome SHP-2/Ptpn11 mutants enhance calcium oscillations and impair NFAT signaling. *Proc Natl Acad Sci U S A.* 2006;103:2160-2165. doi:10.1073/pnas.0510876103
53. Tartaglia M, Mehler EL, Goldberg R, et al. Mutations in PTPN11, encoding the protein tyrosine phosphatase SHP-2, cause Noonan syndrome. *Nat Genet.* 2001;29:465-468. doi:10.1038/ng772
54. Kroisel PM, Häusler M, Klaritsch P, et al. Targeted enrichment sequencing in two midterm pregnancies with severe abnormalities on ultrasound. *Lancet.* 2017;389:1857-1858. doi:10.1016/S0140-6736(17)31049-8
55. Zhang J, Huang J, Qi T, et al. SHP2 protects endothelial cell barrier through suppressing VE-cadherin internalization regulated by MET-ARF1. *FASEB J.* 2019;33:1124-1137. doi:10.1096/fj.201800284R
56. Derivery E, Sousa C, Gautier JJ, Lombard B, Loew D, Gautreau A. The Arp2/3 Activator WASH Controls the Fission of Endosomes through a Large Multiprotein Complex. *Dev Cell.* 2009;17:712-723. doi:10.1016/j.devcel.2009.09.010
57. Sadowski L, Pilecka I, Miaczynska M. Signaling from endosomes: Location makes a difference. *Exp Cell Res.* 2009;315:1601-1609. doi:10.1016/j.yexcr.2008.09.021
58. Tian Y, Gawlak G, O'Donnell JJ, Birukova AA, Birukov KG. Activation of Vascular Endothelial Growth Factor (VEGF) receptor 2 mediates endothelial permeability caused by cyclic stretch. *J Biol Chem.* 2016;291:10032-10045. doi:10.1074/jbc.M115.690487
59. Miquerol L, Langille BL, Nagy A. Embryonic development is disrupted by modest increases in vascular endothelial growth factor gene expression. *Development.* 2000;127:3941-3946.
60. Le Cras TD, Spitzmiller RE, Albertine KH, Greenberg JM, Whitsett JA, Akeson AL. VEGF causes pulmonary hemorrhage, hemosiderosis, and air space enlargement in neonatal mice. *Am J Physiol - Lung Cell Mol Physiol.* 2004;287:134-42. doi:10.1152/ajplung.00050.2004
61. Smith GA, Fearnley GW, Tomlinson DC, Harrison MA, Ponnambalam S. The cellular response to vascular endothelial growth factors requires co-ordinated signal transduction, trafficking and

- proteolysis. *Biosci Rep*. 2015;35:e00253. doi:10.1042/BSR20150171
62. Peterson T, Kirkpatrick N, Huang Y, et al. Tmic-07. Dual Inhibition of Ang-2 and Vegf Receptors Normalizes Tumor Vasculature and Prolongs Survival in Glioblastoma By Altering Macrophages. *Proc Natl Acad Sci U S A*. 2016;113:4470-5. doi: 10.1073/pnas.1525349113.
 63. Kang S, Park KC, Yang KJ, Choi HS, Kim SH, Roh YJ. Effect of cediranib, an inhibitor of vascular endothelial growth factor receptor tyrosine kinase, in a mouse model of choroidal neovascularization. *Clin Exp Ophthalmol*. 2013;41:63-72. doi:10.1111/j.1442-9071.2012.02813.x
 64. Bauditz J, Lochs H. Angiogenesis and vascular malformations: Antiangiogenic drugs for treatment of gastrointestinal bleeding. *World J Gastroenterol*. 2007;13:5979-5984. doi:10.3748/wjg.13.5979
 65. Araki T, Mohi MG, Ismat FA, et al. Mouse model of Noonan syndrome reveals cell type- and gene dosage-dependent effects of Ptpn11 mutation. *Nat Med*. 2004;10:849-857. doi:10.1038/nm1084
 66. Steklov M, Pandolfi S, Baietti MF, et al. Mutations in LZTR1 drive human disease by dysregulating RAS ubiquitination. *Science*. 2018;362:1177-1182. doi:10.1126/science.aap7607
 67. Li B, Dewey CN. RSEM: Accurate transcript quantification from RNA-seq data with or without a reference genome. *Bioinforma Impact Accurate Quantif Proteomic Genet Anal Res*. 2014:41-74. doi:10.1201/b16589



Circulation Research

FIGURE LEGENDS

Figure 1. Loss of *Lztr1* leads to vascular defects during embryogenesis. (a) Representative images of *Lztr1*^{+/+}, *Lztr1*^{+/-}, and *Lztr1*^{-/-} embryos at E14.5. The arrowhead indicates hydrops. Scale bar 1 mm. Size of E14.5 embryos is shown as mean ± SEM; p-values were assessed by Kruskal-Wallis test with Dunn's Multiple Comparison Test. (b) H&E-stained sections of the back skin of E14.5 *Lztr1*^{+/+}, *Lztr1*^{+/-}, and *Lztr1*^{-/-} embryos. Arrowheads indicate hemorrhages; arrows denote dermis thickness. Scale bar 200 µm. (c) Representative images of *Lztr1*^{fl/fl} and *Pdgfb*^{iCreERT2}, *Lztr1*^{fl/fl} embryos at E14.5. The arrowhead indicates nuchal translucency. Scale bar 1 mm. Size of E14.5 embryos is shown as mean ± SEM; p-values were assessed by Wilcoxon-Mann-Whitney test. (d) H&E-stained sections of the head of *Lztr1*^{fl/fl} and *Pdgfb*^{iCreERT2}, *Lztr1*^{fl/fl} embryos at E14.5. Scale bar 100 µm (e) H&E-stained sections of *Lztr1*^{+/+}, *Lztr1*^{+/-} and *Lztr1*^{-/-} yolk sacs. * indicates enlarged vascular structure. Scale bar 200 and 500 µm, respectively. (f) 3D vasculature of brain (cephalic plexus) imaged after whole mount-staining of E14.5 embryos with Isolectin B4 (IB4), mouse iG (miG), and clearing. Scale bar 200 µm.

Figure 2. Loss of *Lztr1* leads to pulmonary vascular disease. (a) Gross anatomy and H&E-staining of lungs of 52-week old *Lztr1*^{+/+} and *Lztr1*^{+/-} mice. Scale bar 500 µm. * indicate bronchioles; pulmonary vessels are delineated in red. (b) Masson Trichrome-stained sections of *Lztr1*^{+/+} and *Lztr1*^{+/-} lungs. Fibrosis is colored in blue. Scale bar 500 µm. (c) Fibrotic area in lungs of 52-week old *Lztr1*^{+/+} and *Lztr1*^{+/-} mice. Data are shown as mean ± SEM; p-values were assessed by Wilcoxon-Mann-Whitney test. (d) H&E-staining of lungs of 10-week old *Lztr1*^{+/+} and *Lztr1*^{+/-} mice. Scale bar 500 µm. Hemorrhagic area is shown as mean ± SEM; p-values were assessed by Wilcoxon-Mann-Whitney test. (e) Lungs of 52-week old *Lztr1*^{+/+} and *Lztr1*^{+/-} mice immunostained with anti-SMA and anti-CD31 antibodies. Data are shown as mean±SEM; p-values were assessed by Wilcoxon-Mann-Whitney test. Scale bar 20 µm. (f) ECs isolated from *Lztr1*^{+/+} and *Lztr1*^{+/-} mice immunostained with antibodies against VE-cadherin and ZO1. Blue rectangles delineate the magnified areas (below). Data are shown as mean ± SEM; p-values were assessed by Wilcoxon-Mann-Whitney test. Scale bar 20 µm. (g) Evans blue extravasation from lungs of *Lztr1*^{+/+} and *Lztr1*^{+/-} mice. Lines shows mean; p-values were assessed by Wilcoxon-Mann-Whitney test. (h) Evans blue extravasation from *Lztr1*^{fl/fl} and *Pdgfb*^{iCreERT2}, *Lztr1*^{fl/fl} tissues. Lines shows mean; p-values were assessed by Wilcoxon-Mann-Whitney test. (i) Paracellular permeability of *Lztr1*^{+/+} and *Lztr1*^{+/-} ECs as measured by quantifying FITC Dextran fluorescence in a trans-well assay. P-values were assessed by two-way ANOVA with Bonferroni post-tests.

Figure 3. *Lztr1* loss affects vesicular trafficking. (a) IPA analysis of differentially expressed proteins in HeLa cells harboring wt-LZTR1 or LZTR1-indels. Differentially expressed proteins were identified by MS-based shot gun analysis using the FDR approach. N=3 (b) IPA analysis of differentially ubiquitinated peptides in HeLa cells harboring wt-LZTR1 or LZTR1-indels. GG-modified peptides were captured by anti-K-ε-GG antibody and quantified by MS. Differentially ubiquitinated proteins were identified by the FDR approach. N=3 (c) Putative LZTR1 interactors identified by the Virotrap approach as described in Steklov et al., 2018. Endocytosis-related proteins are shown in red. N=3 (d, e) *Lztr1*^{fl/fl} ECs expressing an empty vector (EV) or Cre recombinase were immunostained with anti-SNX1 antibody. Scale bar 10 µm. Each dot shows mean value for 25 ECs isolated from one mouse. Lines show mean±SEM; p-values were assessed by Wilcoxon-Mann-Whitney test. Sphericity ranges from 0 to 1 indicating if the structures are spheric (close to 1) or more tubular (close to 0.5). (f, g) *Lztr1*^{fl/fl} ECs transduced with an empty vector (EV) or Cre-recombinase coding virus (Cre) were treated with DMSO, Dynasore (40µM), or TyrA23(10µM) for 12 hours and immunostained with anti-ZO1 and anti-VE-cadherin antibody. Scale bar 20 µm. Quantification of the number of junctional gaps per cells. N=4; 25 cells per group were analyzed; p-values were assessed by Kruskal Wallis test with Dunn's Multiple Comparison Test (h) Progeny from *Lztr1*^{+/-} matings at E18.5 and after birth in a mock group or a Dynasore-treated group (1mg/kg; starting from E2.5). P-values were calculated using Fisher Exact test.

Figure 4. LZTR1 regulates CHMP1B ubiquitination. (a) Ubiquitinome analysis of wt-LZTR1 or LZTR1-indel HeLa cells. N=3. For each protein, log₂ (fold change between both conditions) is plotted vs Fold Change Rank. CHMP1B ubiquitination sites are shown in red. (b, c) An empty vector (EV), HA-tagged wt-LZTR1, or LZTR1 mutants were overexpressed in HeLa cells. Endogenous CHMP1B was immunoprecipitated using anti-CHMP1B antibody conjugated to agarose. The amount of pulled-down LZTR1 was detected by immunoblotting with anti-HA antibody. (d) CHMP1B was pulled down from ECs expressing HA-wt-LZTR1 using an anti-CHMP1B antibody. The amount of pulled-down HA-wt-LZTR1 was detected by immunoblotting. (e) Ubiquitinated proteins were immunoprecipitated from *Lztr1*^{+/+} and *Lztr1*^{+/-} ECs isolated using anti-ubiquitin FK2 antibody. The amount of pulled-down CHMP1B was detected by immunoblotting. (f) Ubiquitinated proteins were immunoprecipitated from ECs treated with VEGF (100ng/ml, 30 minutes) or MLN4924 (1μM, 12hours) using anti-Ubiquitin FK2 antibody. The amount of pulled-down CHMP1B was detected by immunoblotting. (g) Ubiquitinated proteins were immunoprecipitated from HeLa cells with *Lztr1*-indel overexpressing empty vector (EV), wt-LZTR1, or NS-associated LZTR1 mutants using anti-ubiquitin FK2 antibody conjugated to agarose. The amount of pulled-down CHMP1B was detected by immunoblotting. * indicates ubiquitinated CHMP1B.

Figure 5. LZTR1-mediated CHMP1B ubiquitination modulates vesicle trafficking. (a) Immunostaining of *Lztr1*^{+/+} and *Lztr1*^{+/-} ECs transfected with a Scrambled siRNA or siRNA targeting Chmp1b with antibodies against RAB11, CHMP1B and VEGFR2. Scale bar 20 μm. (b) Quantification of endosomal RAB11 levels in *Lztr1*^{+/+} and *Lztr1*^{+/-} ECs transfected with a Scrambled siRNA or siRNA targeting Chmp1b. Data shown as mean ± SEM; p-values were assessed by Wilcoxon Mann-Whitney test. >25 cells per mice were analyzed. (c) *Lztr1*^{fl/fl} ECs expressing an empty vector (EV) or Cre recombinase were immunostained with the indicated antibodies. Scale bar 10 μm. (d) ECs isolated from *Lztr1*^{+/+} and *Lztr1*^{+/-} mice immunostained with the indicated antibodies. Scale bar 10μm. (e) Quantification of colocalization of CHMP1B and endosomal markers in *Lztr1*^{+/+} and *Lztr1*^{+/-} ECs is shown as mean ± SEM; p-values were assessed by Wilcoxon-Mann-Whitney test. 25 cells per mice were analyzed. (f) An empty vector (EV), V5-tagged wt-CHMP1B, or CHMP1B-7K>R mutant was overexpressed in wt-LZTR1 or LZTR1-indels HeLa cells expressing sh CHMP1B. Quantification of endosomal RAB11 is shown as mean ± SEM; p-values were assessed by Wilcoxon Mann-Whitney test. N=4.

Figure 6. LZTR1-mediated VEGFR2 internalization affects blood vessel integrity. (a, b) *Lztr1*^{fl/fl} ECs were infected with an empty vector (EV) or Cre-recombinase (Cre) and treated with DMSO, Dynasore (40μM), or TyrA23(10μM) for 12 hours. After permeabilization, the cells were immunostained with anti-VEGFR2 antibody. Scale bar 20 μm. Data shown as mean ± SEM; p-values were assessed by Wilcoxon Mann-Whitney test. (c) Levels of internalized VEGFR2 were assessed by immunostaining of *Lztr1*^{+/+} and *Lztr1*^{+/-} ECs transfected with Scrambled siRNA or siRNA targeting *Chmp1b*. Data are presented as mean ± SEM; p-values were assessed by Wilcoxon Mann-Whitney test. (d) ELISA analysis of soluble VEGFR2 in the plasma of *Lztr1*^{+/+} and *Lztr1*^{+/-} mice. Data are present as mean ± SEM; p-values were assessed by Wilcoxon Mann-Whitney test. (e, f) Immunoblotting analysis of phosphorylated and total VEGFR2 in *Lztr1*^{fl/fl} ECs infected with an empty vector (EV) or Cre-recombinase (Cre) and treated with DMSO, MLN4924 (1μM), or Tyrphostin A23(10μM) for 12 hours. Data shown as mean ± SEM; p-values were assessed by Mann-Whitney test. (g, h) *Lztr1*^{fl/fl} ECs transduced with empty vector (EV) or Cre-recombinase (Cre), treated for 12 hours with DMSO or cediranib (10μM), and immunostained with antibodies against ZO1 and VE-cadherin. Scale bar 20 μm. Quantification of the number of cells with junctional gaps is shown as mean ± SEM; p-values were assessed by Wilcoxon Mann-Whitney test to compare efficiency of each specific treatment within each group. (i) Evans blue extravasation from *Pdgfb*^{iCreERT2}, *Lztr1*^{fl/fl} and *Lztr1*^{fl/fl} mice skin after treatment with PBS or VEGF. Miles assay performed on the ears. N=4 mice per group. Data are normalized to tissue weight and shown as mean ± SEM; p-values were assessed by Wilcoxon Mann-Whitney test to compare efficiency of treatment within group. (j) Evans blue extravasation from *Pdgfb*^{iCreERT2}, *Lztr1*^{fl/fl} and *Lztr1*^{fl/fl} mice skin after vehicle or cediranib treatment. Miles assay. N=4 mice per group.

Data are normalized to tissue weight and shown as mean \pm SEM; p-values were assessed by Wilcoxon-Mann-Whitney test to compare efficiency of treatment within group.



Circulation Research

NOVELTY AND SIGNIFICANCE

What Is Known?

- The Noonan Syndrome gene LZTR1 determines substrate specificity of the CULLIN3 ubiquitin ligase complexes.
- Cardiac injury and bleeding disorders have been recently described in Noonan Syndrome patients harboring LZTR1 mutations.
- Currently, there are no therapeutic options for the management of bleeding complications in Noonan Syndrome patients.

What New Information Does This Article Contribute?

- Loss of Lztr1 in mice leads to endothelial dysfunction that phenotypically overlaps with bleeding pathologies observed in Noonan Syndrome patients.
- LZTR1 affects the dynamics of vesicle trafficking by controlling ubiquitination of the ESCRT-III component CHMP1B.
- Lztr1-mediated dysregulation of CHMP1B ubiquitination triggers endosomal accumulation and subsequent activation of VEGFR2, causing disruption of endothelial junctions and bleeding.



Our findings provide a fundamental explanation underlying the molecular mechanism of endothelial dysfunction in Noonan Syndrome patients harboring LZTR1 mutations. By combining comprehensive analysis of Lztr1 knockout models and unbiased proteomics and transcriptomics approaches, we demonstrated that loss of Lztr1 function leads to vascular dysfunction by dysregulating vesicular trafficking and subsequent activation of VEGFR2. Our results indicate that ELISA screening of Noonan Syndrome patients for the levels of soluble VEGFR2 in blood plasma may predict both the severity of Noonan Syndrome phenotypes and potential responders to anti-VEGF therapy, whereas anti-VEGF therapies such as cediranib could be a potential treatment approach for managing bleeding disorders in LZTR1-mutated Noonan Syndrome patients.

Figure 1

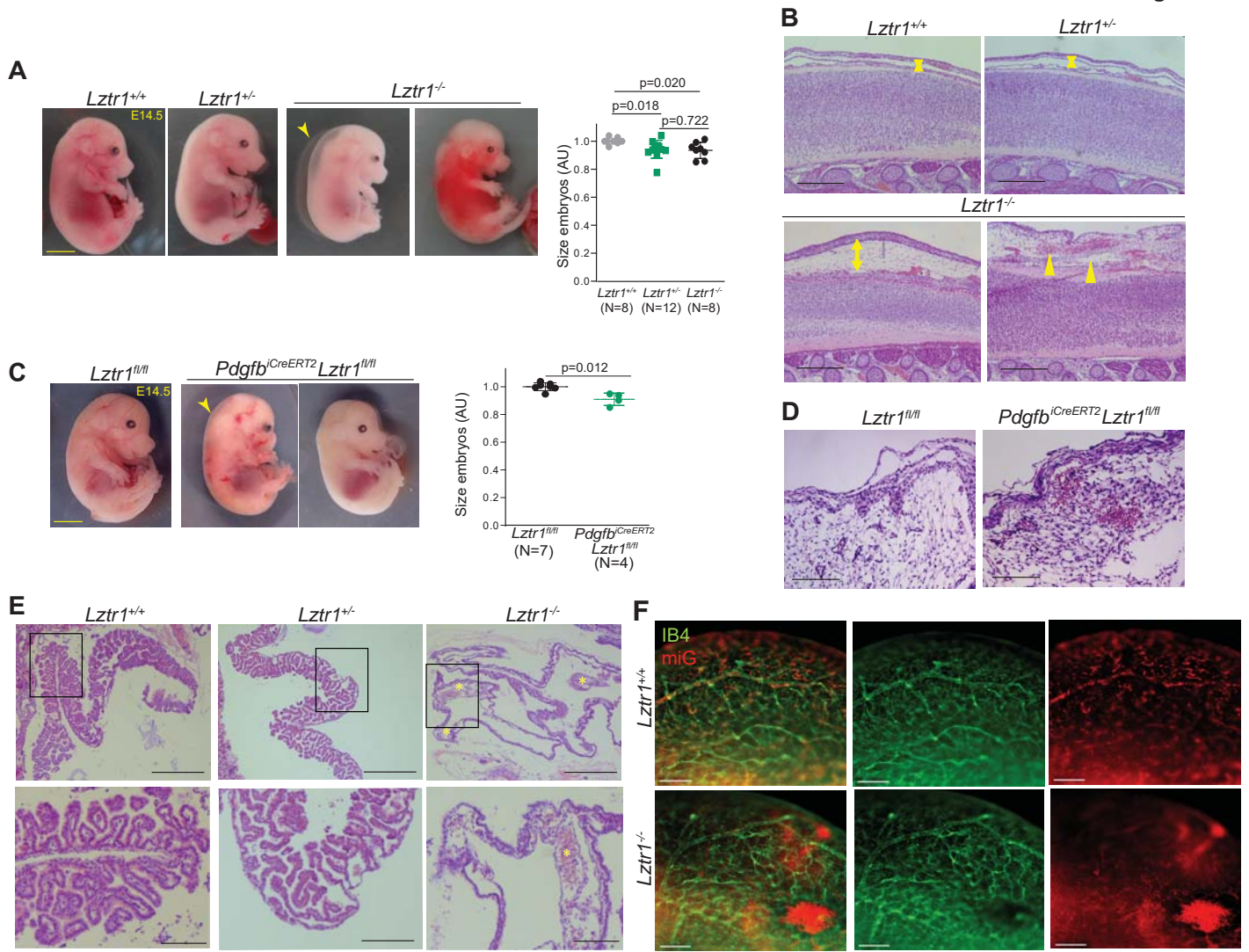


Figure 2

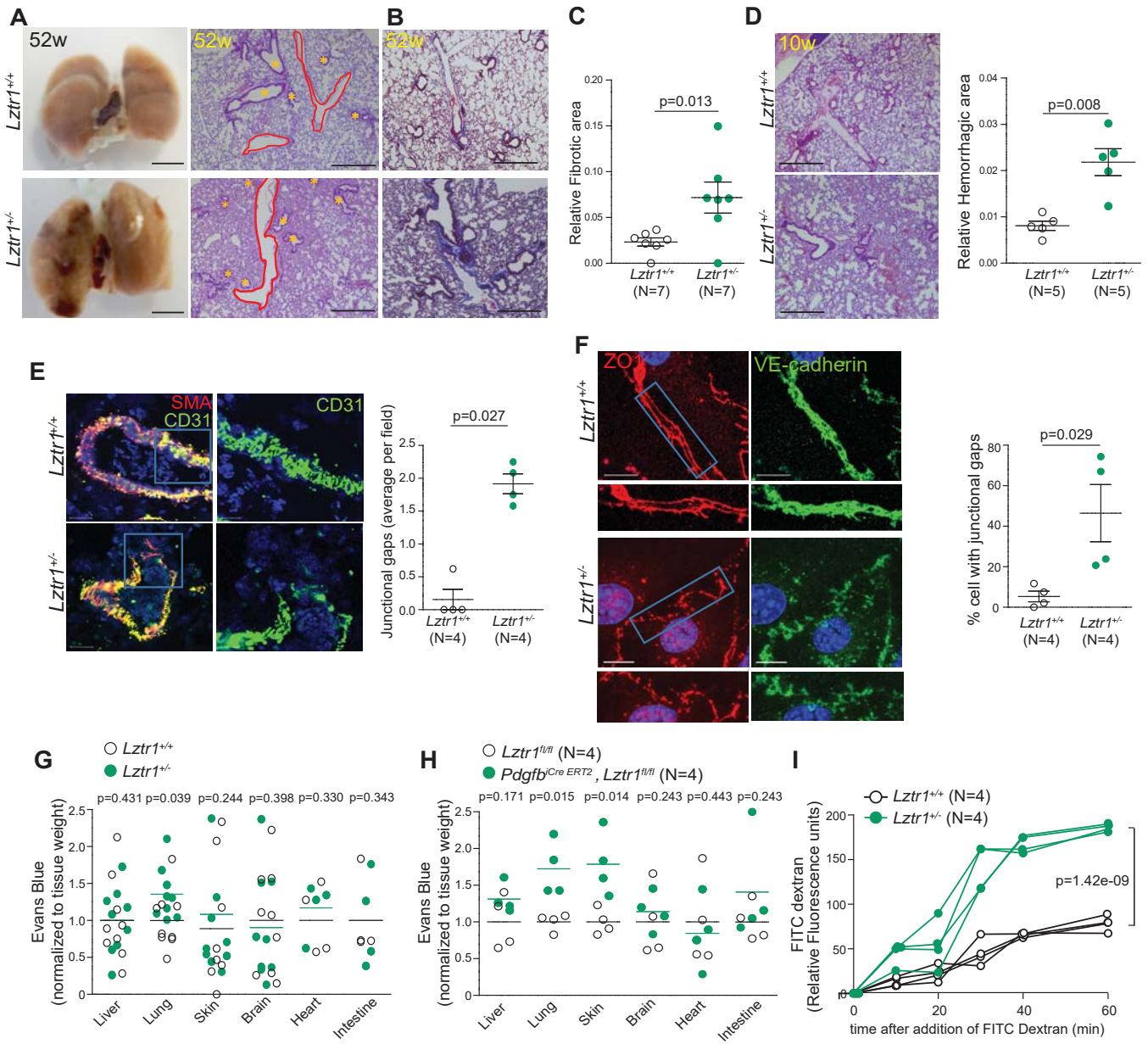


Figure 3

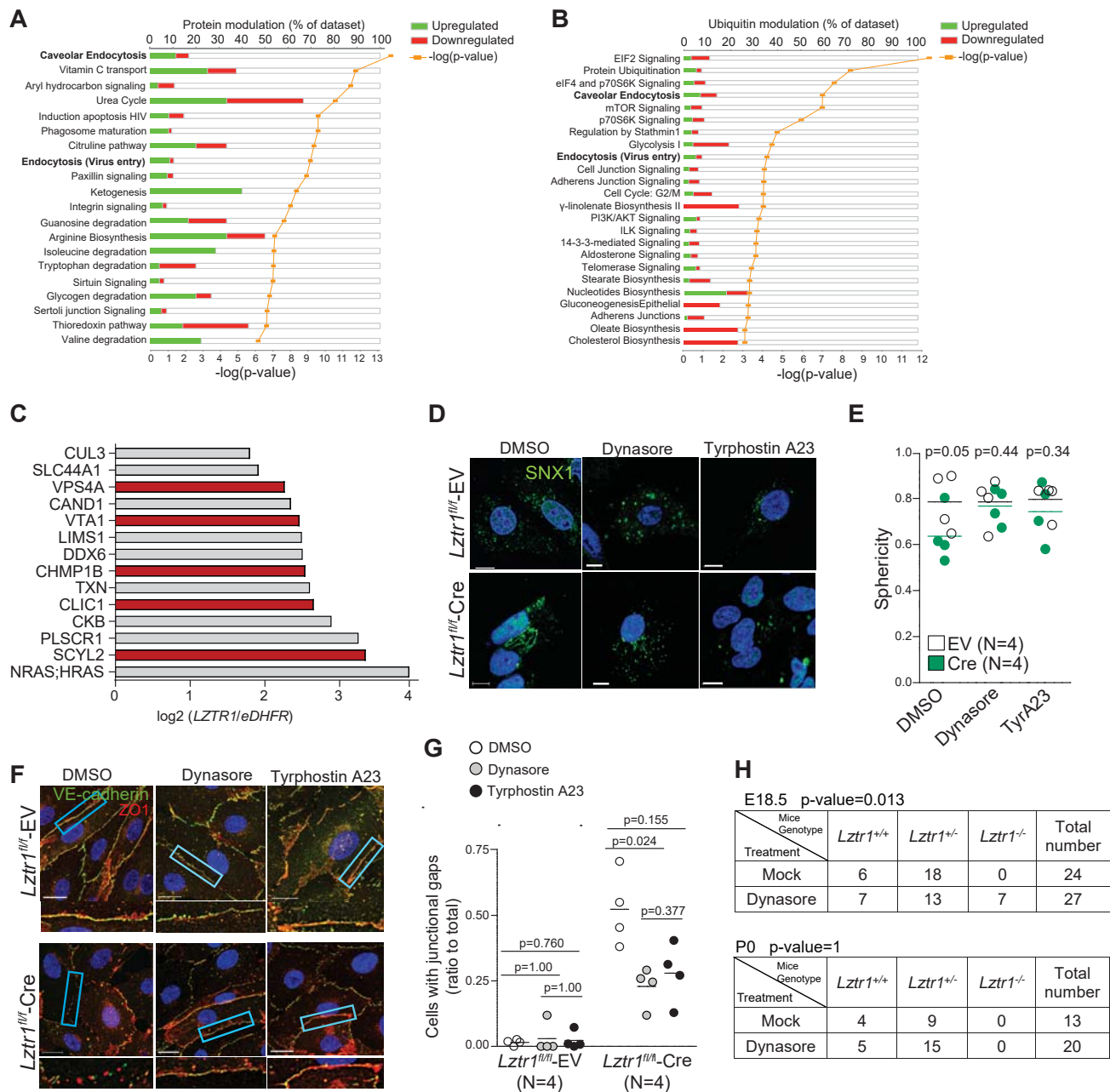


Figure 4

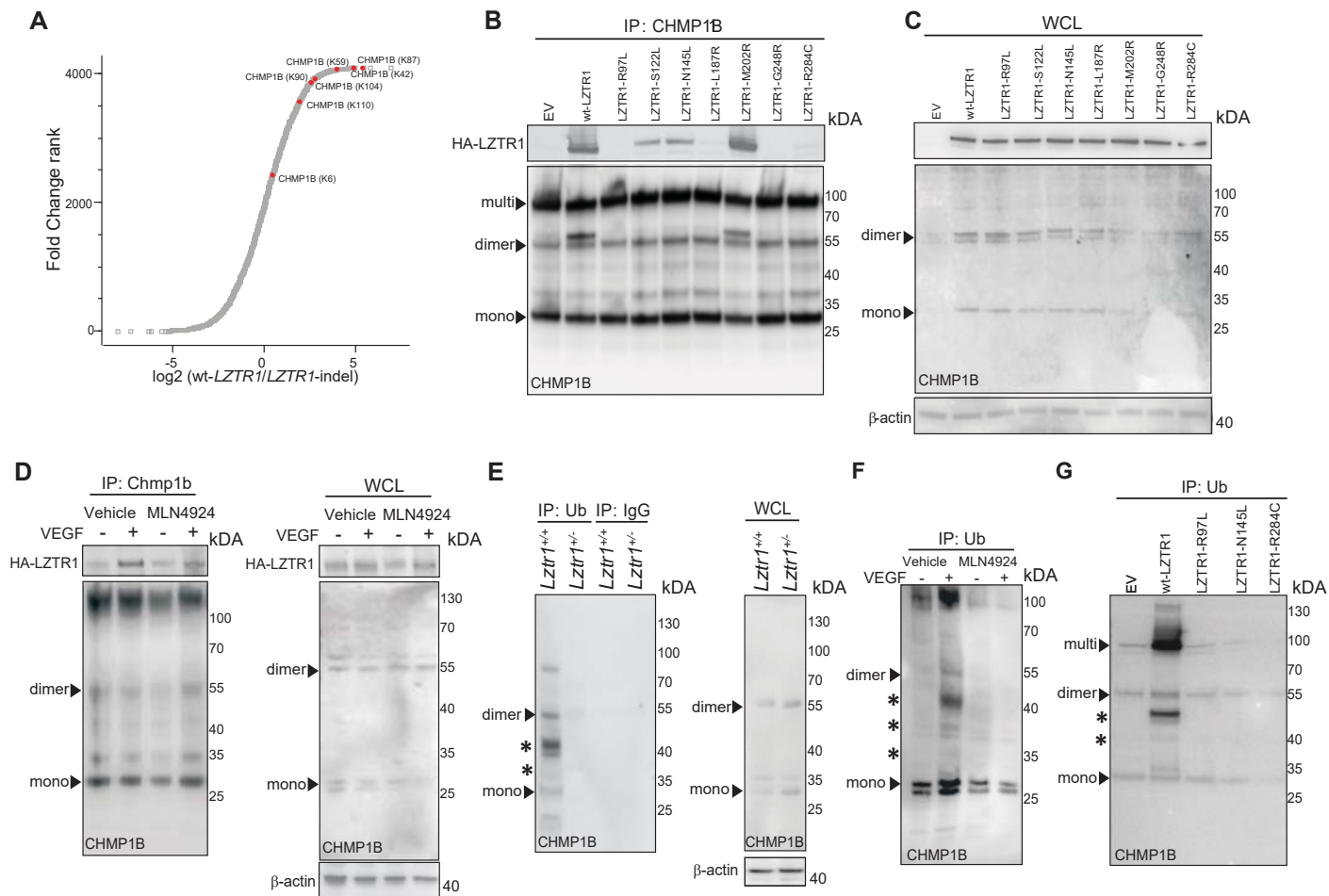


Figure 5

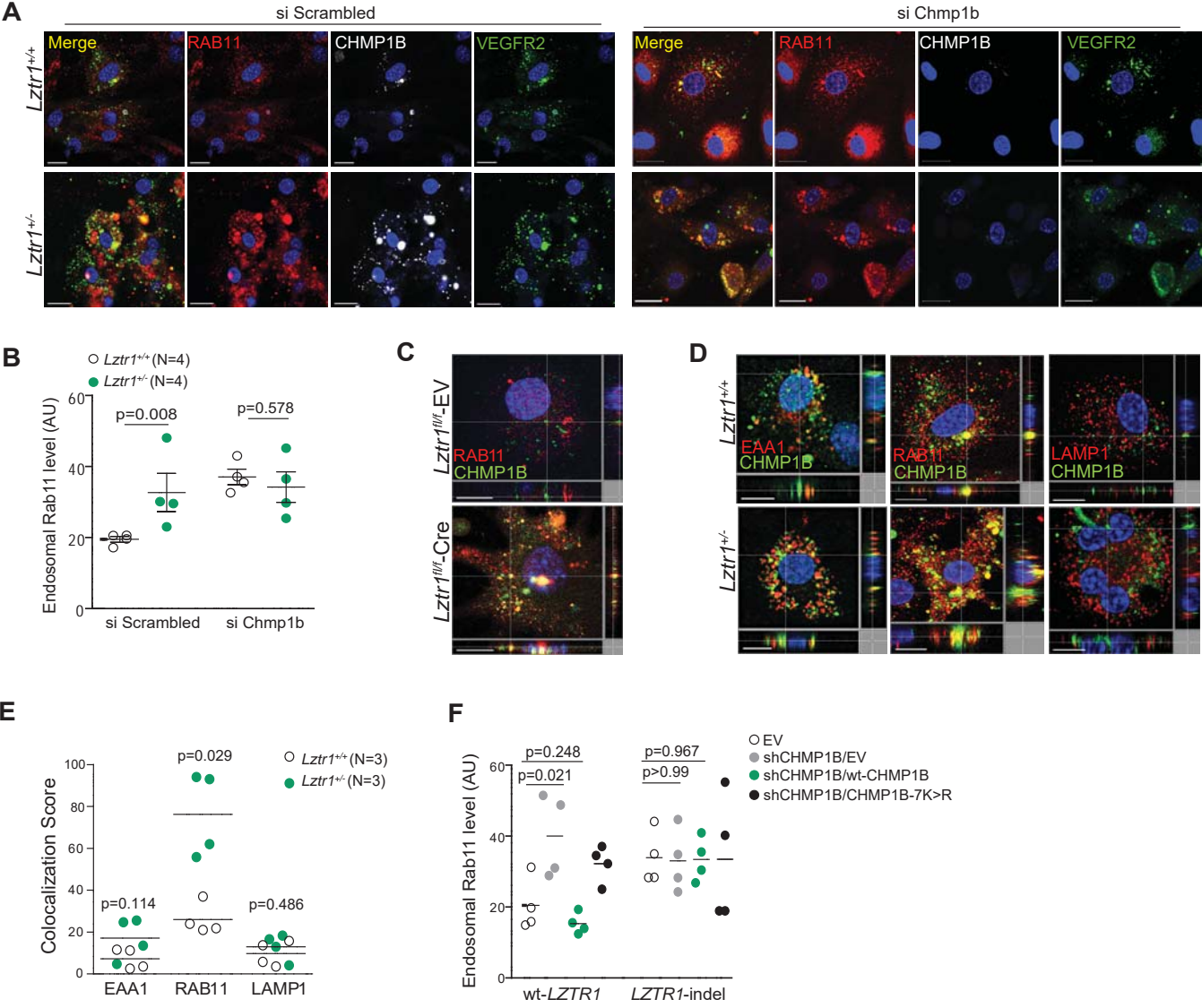


Figure 6

